# Influence of dissolution on frictional properties of carbonate faults

**H. Rattez[1], F. Dissidoro[2], J. Sulem[3], M. Veveakis[1]**

[1]Civil and Environmental Engineering, Duke University, Durham, NC, USA

[2]Department of Structural, Building and Geotechnical Engineering, Politecnico di Torino, Torino, Italy

[3]Laboratoire Navier UMR8205, CNRS, ENPC & IFSTTAR, Université Paris-Est, Marne La Vallée, France

Corresponding author: Hadrien Rattez (hadrien.rattez@duke.edu)

## Highlights

- Velocity stepping experiments are conducted for a synthetic calcite gouge with an annular shear apparatus to study the effect of the injection of an acid fluid.
- Results show a weakening of the carbonate gouge Rate and State parameters, due to acid dissolution and confining stress.
- This weakening is due to the loss of small particles and not the change of rugosity of the grains.
- A modification of the rate and state friction law is proposed to take into account these effects and determine the conditions of fault reactivation in potential injection sites.

**Keywords:** Fault stability; Induced seismicity; Chemo-mechanical couplings; Rate and state friction; $CO_2$ storage; Acid gas injection

**Abstract**

Velocity stepping experiments have been performed on a simulated calcite gouge using an annular shear apparatus to investigate the effect of dissolution on the frictional properties of a carbonate fault. The tested material was put in contact with hydrochloric acid at different concentration in order to dissolve the grains. Particle size analysis shows that the small grains tend to disappear due to the chemical reaction, whereas the large grains are not much affected. The dissolution process mainly induces a decrease of the fractal number of the grain size distribution. The study of the rate-and-state parameters of the gouge, which enables to characterize the ability of the fault to generate earthquakes, shows a weakening due to the dissolution and the confining stress. This weakening implies that faults can become seismogenic after the injection in a carbonate reservoir of an acid fluid. This effect is explained by the removal of small particles, countering the increase of rugosity of the grains. Based on the experimental results, a constitutive law is suggested, in order to capture the influence of dissolution and confining stress on the frictional properties of fault. It enables to determine in which conditions of maturity and degradation of a fault and at which depth, a seismic slip can be triggered by anthropogenic activities like acid/CO2 injection.

## 1. Introduction

A variety of human activities can modify the stress state or the material properties of underground rocks and, thus, induce an instability at the origin of an earthquake. The anthropogenic cause of seismicity has been shown for different types of projects. The most commonly reported anthropogenic activities to have induced earthquakes are Mining and water reservoir impoundment, but it can also be caused by fracking, oil and gas extraction, waste water disposal or geothermal projects (Wilson et al. 2017). Human-made tremors have drastically increased in the U.S. since 2001 from a previous average of 21 quakes a year to 188 documented in 2011 (Ellsworth 2013). For instance, infrastructures and people in Oklahoma and southern Kansas face potential damages in the next years from induced earthquakes, in a similar level to regions known for their large number of natural earthquakes, like southern California (Schoenball and Ellsworth 2017). However, induced earthquakes are usually not a threat for human life, because they have a maximum magnitude of 3-4 and for constructions obeying the actual codes they would not be a root of damages (Zoback and Gorelick 2012).

A large number of numerical studies have been devoted to study the mechanisms at the origin of induced seismicity and to evaluate the maximum magnitude of the earthquake a project may induce (Cappa 2012). Most of them consider a hydro-mechanical model and look at the modifications of the stress state at the location of a known fault in a specific site (Baisch et al. 2010; Yehya, Yang, and Rice 2018; Mortezaei and Vahedifard 2015; Cappa 2012). In these studies, fluid injection into a reservoir-caprock system bounded by a fault is modelled with different stress state conditions and assuming various permeability. The time of appearance of the first potential earthquake can be computed and the value of the stress drop permits to estimate the magnitude.

Projects like acid gas disposal, enhanced oil recovery or carbon capture and storage involve the injection of a reacting fluid into a reservoir (Khan, Amin, and Madden 2013).The Carbon Capture and Storage (CCS) is one of the methods considered to reduce emissions of $CO_2$ into the atmosphere (Espinoza 2011). The principle is to capture the $CO_2$ and separate it from other gases in the combustion smoke of significant plants like cement factories or coal-burning power plants. Once extracted, the gas is compressed and transported with a pipeline to injections sites for long term storage. Acid gas disposal is a method used by oil and gas producer to reduce atmospheric emissions of hydrogen sulphide ($H_2S$). A mixture of hydrogen sulphide and carbon dioxide (by-product of 'sweetening' sour hydrocarbons) is injected into depleted reservoirs or deep saline aquifers (Bachu and Gunter 2004). Enhanced oil recovery, also called tertiary recovery, is a way to improve the extraction of crude oil from reservoir that could not be extracted otherwise (Rubinstein and Mahani 2015). The most common methods are gas or chemical injection that modifies the viscosity of the oil and improve its mobility. In these cases, induced seismicity could produce damage to the well or the caprock and deteriorate the sealing of the reservoirs, leading to the failure of the project.

The injection of an acid does not only change the stress state, but also modifies the properties of the storage medium. Some theoretical studies and observations have looked at the influence of chemical reactions on the potential of a fault to create earthquakes. (Yarushina and Bercovici 2013) have looked at the effect of supercritical $CO_2$ on mafic rocks. The reaction of carbonatation that happens between the minerals and the carbon creates products that will precipitate on the surface of grains leading to an increase of their diameter. In the same time, the pore pressure will decrease because the fluid will be consumed by the reaction. They conclude that all these phenomena will prevent the triggering of earthquakes if the injection rate is not too high. On the contrary, (Collettini et al. 2008) have shown that the presence of $CO_2$ can destabilize a preexisting fault. After analyses of samples issued from a site in northern Apennines, they discovered that there is a degassing of a trapped bubble of $CO_2$ under the fault, that operates as a weakening process. In the long term, the fluid reacts with fine grains in the fault gouge to change the mineralogy and produce weak, phyllosilicate-rich fault rocks that deform with a very low friction coefficient, facilitating a seismic slip along the fault.

In this work, we perform experiments in carbonate fault gouges at different dissolution degrees and different confining pressures to assess the effect of long-term exposure of a carbonate to an acid fluid. The combined effects of dissolution and confinement are then used to produce a chemo-mechanical enhancement in the classical rate-and-state friction law, and the critical operational conditions to avoid induced seismicity in a carbonate-rich fault are discussed.

## 2. Experimental setup

### 2.1. Materials

The material used for the experiments is a carbonate sand extracted from the Fergues quarry by the company "les Carrières du Boulonnais" located in the North of France. The sand is composed of 99% of calcite ($CaCO_3$) and show traces of quartz ($SiO_2$), magnesium carbonate ($MgCO_3$), Hematite ($Fe_2O_3$) and Aluminium Oxide ($Al_2O_3$). The grain size distribution is obtained using a combination of sieves and hydrometer analysis or laser diffraction. Both methods show similar results and the broad size distribution of the material is shown in Figure 1.

Some samples of the sand are put in contact with a solution of water and hydrochloric acid, which is a strong acid, to simulate the long-term effect of dissolution by a weak acid like carbonic acid on the grain size distribution. The reason for using this acid, instead of carbonic acid or other acids, corresponding to the fluid injected in the case of acid gas injection or enhanced oil recovery is that the kinetics of the chemical reaction is almost instantaneous. The calcium carbonate ($CaCO_3$) is dissolved by the hydrochloric acid (HCl) and the products of reaction are carbon dioxide ($CO_2$), water ($H_2O$) and calcium chloride ($CaCl_2$). The equation of the reaction is:

$$\mathrm{CaCO_3^{(s)}} + \mathrm{2HCl^{(l)}} \rightarrow \mathrm{CaCl_2^{(aq)}} + \mathrm{H_2O^{(l)}} + \mathrm{CO_2^{(g)}}.$$

$CaCl_2$ is highly soluble and the specimen are washed several times after the reaction to remove this product of the reaction.

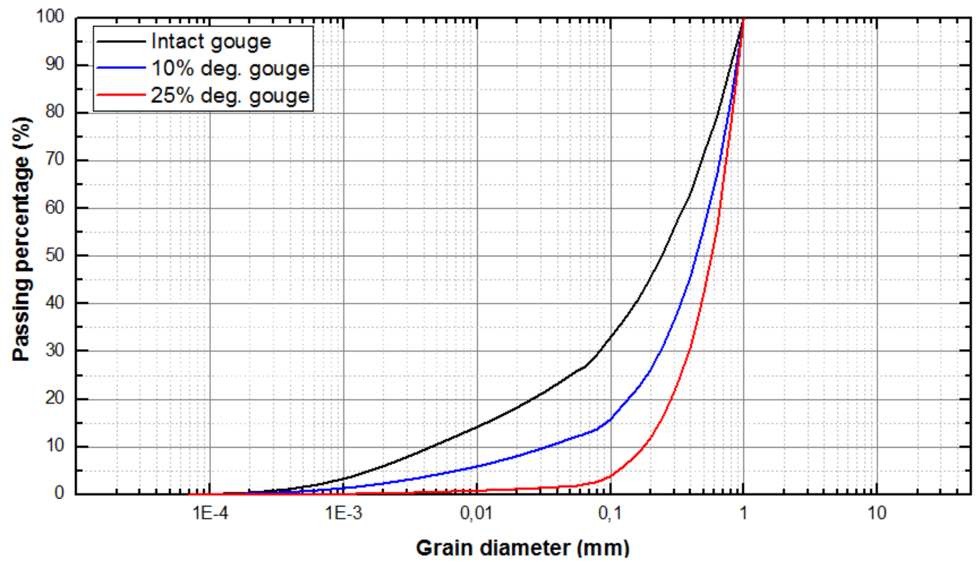


*Figure 1. Cumulative grain size distribution of the simulated fault materials showing different level of dissolution*

The cumulative grain size distributions of the samples for the initial material, after 10% and 25% of dissolution of the total mass are shown in Figure 1. In particular, the higher the degradation, the more the small particles get dissolved, as shown in the next comparison chart. This phenomenon is due to the greater specific surface that small particles offer to the reaction compared to bigger particles.

Considering that our tests are carried out on a material that is supposed to simulate a natural fault gouge, one of the most important material properties to be assessed is the fractal dimension of the grain size distribution. The fractal dimension ($D$) is defined by $N = r^D$, where $N$ is number of particle of diameter $r$. (Sammis, King, and Biegel 1987) measured the particle distribution of intact gouge samples retrieved from the Lopez Fault in the San Gabriel Mountains of Southern California. The gouge is composed mainly of feldspars, quartz and Chlorite, with smaller amounts of calcite and other oxides. The analysis has revealed a remarkable degree of self-similarity for the grain size distribution and the authors have found the fractal dimension to be 1.60 ± 0.11 in two-dimensional cross-section, thus 2.60 ± 0.11 in a three-dimensional volume. On the basis of the observations, they proposed a new model, called the comminution model, for the mechanical processes that generate fault gouges. Self-similarity results from repeated tensile splitting of grains and that splitting probability depends largely on the relative size of nearest neighbors: during the fragmentation process, the direct contact between two particles of near equal size will result in the tensile breakup of one of the two. In this way, at the end of fragmentation process, the material will have a particle distribution in which particles of the same size are separated from each other. Such a spatial organization repeats itself at each scale, providing a self-similar grain distribution having a fractal dimension of 2.58, independently of the initial size distribution of the particles. After the development of this model, several authors conducted experiments on natural and simulated fault gouges, showing their tendency to develop a fractal dimension values of about 2.6 supporting the Sammis' theory (Steacy and Sammis 1991; An and Sammis 1994). However, (Storti, Billi, and Salvini 2003) have analyzed gouge samples of a carbonate fault in the Apennines, Italy and have shown that for this material the comminution model is not always verified. Fractal dimensions obtained from gouges varies from 2.61 to 3.49 in strike-slip faults and from 2.93 to 3.13 in extensional faults. They recognized the value 2.6 to be a threshold between a first stage of fault gouge formation dominated by particles fragmentation and a second one dominated by particles abrasion in the case of carbonate materials.

In Figure 2, the number of particles as a function of the grain diameter is shown for the different level of dissolution of the grains. Only the grain diameters between 0.5μm and 50μm are shown, for better visualization. The value of the fractal number of the sand that is not dissolved is in agreement with the comminution theory and this sand can, therefore, be considered as a good analog of a gouge material. The dissolution induces a decrease of the fractal number from 2.59 to 2.16. This decrease is due to the removal of the small particles from the grain size distribution, in the same way that abrasion makes the fractal number increases due to the creation of more small particles. An interesting feature of the effect of dissolution on the particle size distribution is that it induces an increase of the mean grain diameter. It can, thus, affect the prediction of models considering the mean grain size explicitly like Cosserat continua (Rattez, Stefanou, Veveakis, et al. 2018).

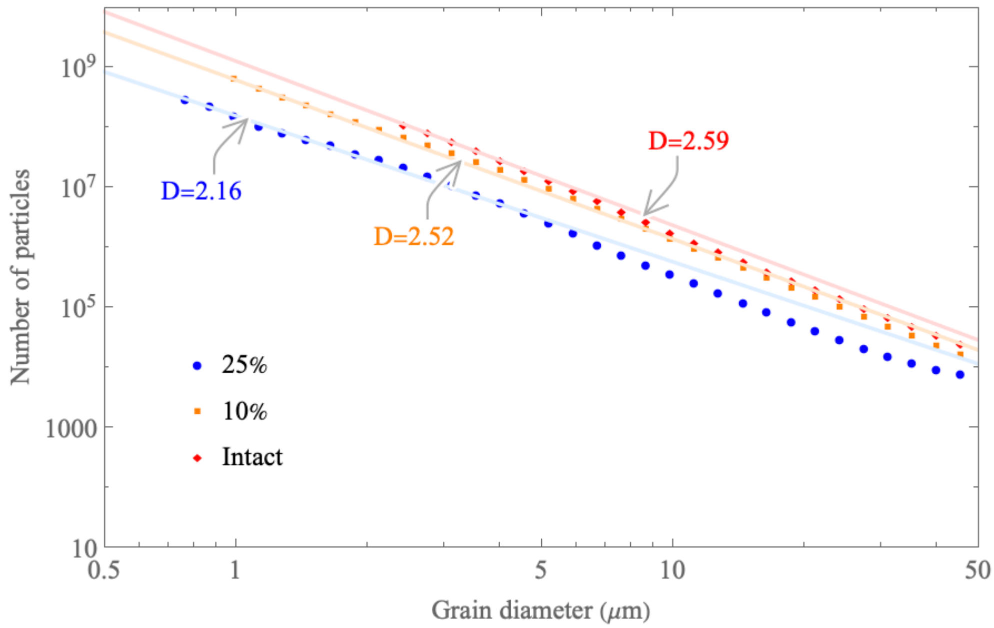


*Figure 2. Number of particles as function of the grain diameter for different level of dissolution of the carbonate sand. The fractal number associated with each distribution is also shown.*

### 2.2. Experimental set-up

The device used for the mechanical tests is an annular simple shear device called ACSA (“Appareil de Cisaillement Simple Annulaire”), designed in 1993 in the CERMES laboratory of Ecole des Ponts (Unterreiner et al. 1993) in order to study the behavior of soil-structure interface. It was then used in the context of fault mechanics by (Chambon, Schmittbuhl, and Corfdir 2006a, 2006b; Messen, Corfdir, and Schmittbuhl 2013). This device enables to shear the gouge material over large displacements and with samples that are thicker than other experimental devices. A cut-away design view of the machine is shown in Figure 3.

The internal surface of a ring-shaped sample, which present a square section of 100mm, is sheared by the rotation of a rough steel cylinder. An optoelectronic rotation encoder is used to monitor the rotation angle of the steel cylinder, and hence the slip distance. The spacing between the triangular striation of the inner interface perpendicular to the sliding direction is 1mm, the same size as the maximum grain diameter of the samples, in order to preclude interfacial slip along the steel-granular boundary (Koval et al. 2011). The outer boundary of the sample is subjected to a constant radial confinement $\sigma_e$ through a 1.5-mm-thick neoprene jacket and applied by a pressure-volume controller. Vertically, the sample is embedded between an upper plate made of duralumin and a lower plate made of glass. All our experiments have been conducted in nominally dry conditions, that is with room atmosphere inside the pore space.

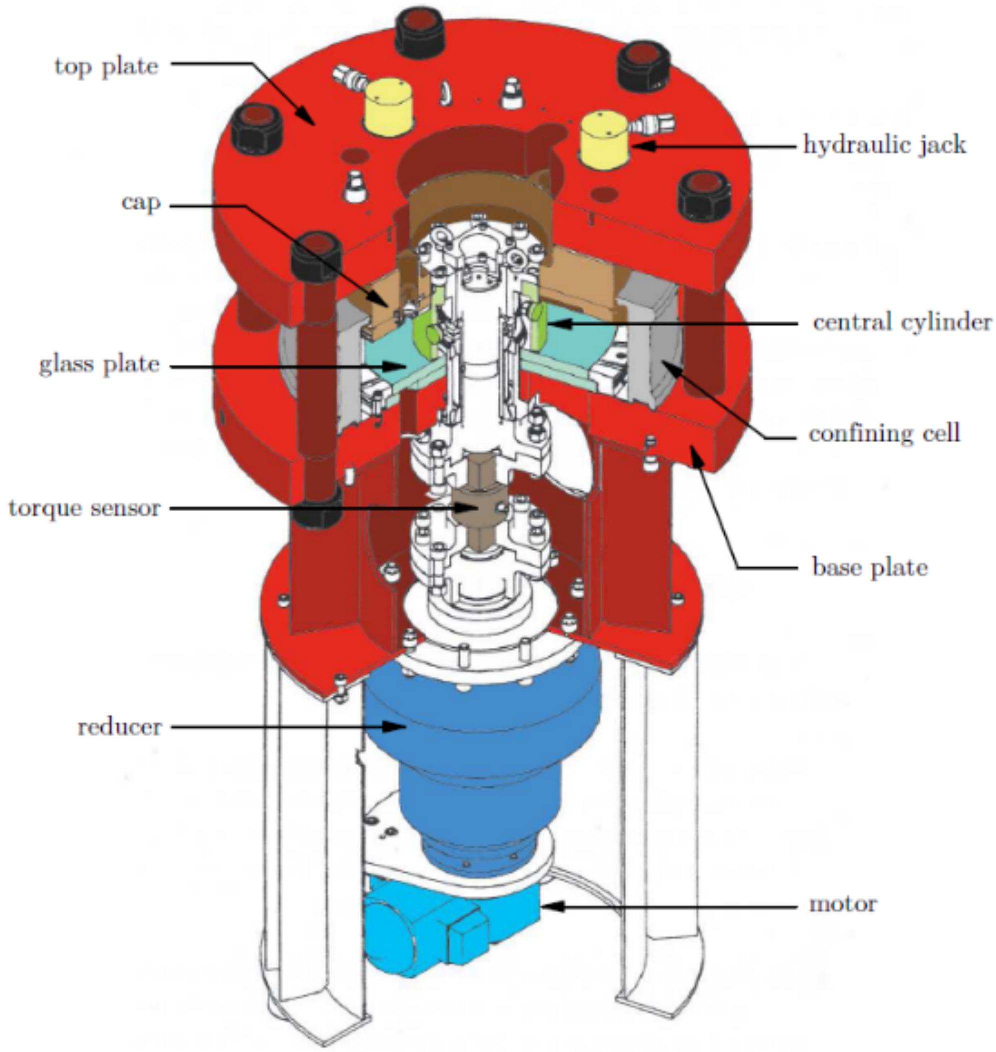


*Figure 3. Cut-away design view of ACSA*

The samples are initially sheared at a constant speed of 2 mm/min for 10 cm, in order to reach the residual friction coefficient. Then, the shearing velocity is abruptly changed every 2 mm of slip to apply different velocity steps. The sequence shown in Table 1 is chosen to repeat every speed step at least two times in order to evaluate the variability of the friction parameters calculated.

| **Stage** | **1** | **2** | **3** | **4** | **5** | **6** | **7** | **8** | **9** |
|---|---|---|---|---|---|---|---|---|---|
| **Displacement** [mm] | 100 | 2 | 2 | 2 | 2 | 2 | 2 | 2 | 2 |
| **Speed** [μm/s] | 33 | 10 | 1.7 | 10 | 33 | 10 | 1.7 | 10 | 33 |

*Table 1. Velocity stepping sequence applied to the sample.*

In Table 2, a list of all the conducted tests with different degrees of dissolution and different confining stresses is presented.

| Degradation | Pressure (kPa) | Test name |
|---|---|---|
| none | 300 | Intact0.6 |
| none | 500 | Intact1 |
| none | 800 | Intact1.6 |
| 10% | 300 | 10deg0.6 |
| 10% | 500 | 10deg1 |
| 10% | 800 | 10deg1.6 |
| 25% | 300 | 25deg0.6 |
| 25% | 500 | 25deg1 |
| 25% | 800 | 25deg1.6 |

*Table 2 – List of complete set of experiments*

## 2.3. Data acquisition and processing

The apparent friction coefficient $\mu$ of the sample is calculated as the ratio of the applied shear stress $\tau$ to the confining stress $\sigma$, $\mu = \frac{\tau}{\sigma}$. The shear stress $\tau$ can be found converting the applied torque measurements $\Gamma$ of the motor:

$$\tau = \frac{\Gamma/r}{A} = \frac{\Gamma/r}{2\pi r H} = \frac{\Gamma}{2\pi r^2 H} \tag{1}$$

where *r* and *H* are respectively the radius and the height of the inner cylinder and are both equal to 10 cm. The pressure exerted on the inner cylinder is different from the external pressure applied on the outer boundary of the sample due to the particular geometry of the sample. According to (Chambon 2003), simple geometrical considerations tend to indicate that the inner normal stress $\sigma_i$ should be equal to twice the applied confinement $\sigma_e$, since the external radius of the sample is the double of the internal one; moreover, the same authors conducted some experiments equipping both the smooth and the rough cylinder with five stress sensors, and they found that normal stress on cylinders' surface was strongly varying at the beginning of the test, but it tended to stabilize after few millimeters of slip toward values very close to the double of external pressure. As the shear band is developing near the inner cylinder, the apparent friction is calculated as:

$$\mu = \frac{\tau}{\sigma_i} = \frac{\Gamma}{2\pi r^2 H} \cdot \frac{1}{2\sigma_e} \quad (2)$$

### 2.4.The Rate-and-State Friction (RSF) law

Since Charles-Augustin Coulomb described the frictional behavior of piece of woods, the understanding of complex microscopic and nanoscopic phenomena underlying has made considerable progress. (Reid 1910) was the first to argue after the 1906 San Francisco earthquake that tremors are not created by the emergence of a new crack in the crust, but rather by the sudden slip along an existing fault. After the beginning of slipping the fault can move seismically or aseismically (Scholz 1998), but this depends on the evolution of friction. A model describing the instability along a fault was developed during the eighties by Dieterich and Ruina (Dieterich 1981; Ruina 1983). They introduced new state variables that describe a second order effect on the coefficient of friction. These laws are called "Rate and State", because the friction depends on the velocity of slipping (Rate) and a state variable θ, which is interpreted as the average lifespan of a set of grain-to-grain contacts in a frictional system. They describe the evolution of the friction coefficient to changes in sliding motions by the equation:

$$\mu = \mu_0 + a \ln\left(\frac{V}{V_0}\right) + b \ln\left(\frac{V_0\,\theta}{D_c}\right) \quad (3)$$

$\mu_0$ is a reference friction coefficient, $V$ and $V_0$ are respectively the actual and reference velocities of the fault. $D_c$ is the characteristic distance of accommodation for friction, associated with the state variable $\theta$. $a$ and $b$ are material properties. This empirical law can capture the phenomenon of stick-slip, which is the name of the instability of friction that creates earthquakes. A simple system called the spring-slider model, in which the slider follows the rate and state friction laws and the spring represents the elastic surrounding mass of the fault, is usually applied to model seismic slips. The study of the linear stability of that system (Rice and Ruina 1983) shows a critical value for the stiffness of the spring $k_{cr}$ (if the inertial terms are negligible). Under this value, the system is unstable and over this value, it is partially stable.

$$k_{cr} = \frac{N}{D_c}(b - a) \quad (4)$$

where $N$ is the normal force applied perpendicular to the direction of sliding. The parameter $(a - b)$ is therefore fundamental to determine the stability of a fault, because if it is positive, instability would never happen.

The parameter $(a-b)$ can be calculated based on the values of friction before and after a sudden velocity change. To evaluate the friction parameter (a-b), the general long-term strain trend of the apparent friction is removed in order to avoid this factor to influence the (a-b) values. It is typically a softening trend as the one shown in Figure 4. The same procedure was also applied by (Samuelson and Spiers 2012) and (Tembe, Lockner, and Wong 2010) during their velocity stepping experiments.

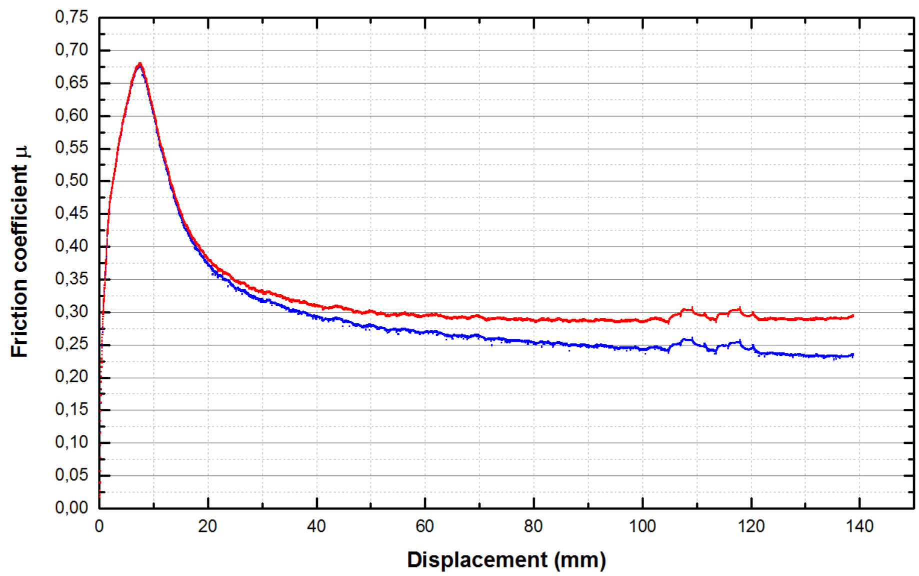


*Figure 4. Friction coefficient line: original (blue) vs straightened (red) (test "intact600").*

The (a-b) value of each velocity step can be obtained from the straightened line of friction coefficient, according to the rate and state friction law:

$$(a-b)=\frac{\mu_0-\mu}{\ln(V/V_0)} \tag{5}$$

where $\mu$ is the coefficient of friction at the end of a step with velocity $V$, and $\mu_0$ and $V_0$ are the coefficient of friction and velocity immediately prior to the velocity step.

## 3. Results

In this section, we describe first the frictional data obtained from the mechanical experiments. The global evolution of the apparent friction as well as the rate and state parameters are presented together with their evolution with confining stress and dissolution, Secondly, the specific surface areas of the samples is assessed by two methods in order to estimate the rugosity of the grains. This analysis is completed with observations obtained using a scanning electron microscope to interpret the different mechanical responses of the samples.

### 3.1.Mechanical results

An example of the apparent friction coefficient evolution with shear displacement is shown in Figure 4. It exhibits a peak for a value between 0.6 and 0.7 for all experiments. This peak is followed by a softening behavior with a characteristic slip distance of a few decimeters, also observed in the experiments performed on glass beads and quartz sand by (Chambon, Schmittbuhl, and Corfdir 2006a).

We observe through the glass window at the bottom of the sample a strain localization of the deformation next to the inner cylinders. The shear band has a thickness of approximately 10 times the mean grain size, in accordance with numerical simulations performed using a Cosserat continuum (Rattez, Stefanou, Sulem, et al. 2018; Rattez, Stefanou, and Sulem 2018).

Regarding the velocity stepping experiments, the results show that all of the tests performed in this study, regardless of degradation level, pressure, exhibit a velocity weakening behavior. The *(a-b)* values are falling between -0.003 and -0.018; the only exception is the 25deg0.6 test, which exhibits the weakest behavior reaching the value of -0.028.

From the slip stability point of view, the general trend is that the dissolution has a weakening effect on the slip stability of tested calcite sand (see Figure 5). All experiments exhibit an unstable behavior ($a\text{-}b<0$), and the dissolution of grains tend to make the values even more negative. Generally, we can see that deg10 results are situated between intact and deg25 ones. It means that a higher degradation induces a higher weakening, and this trend is visible under all pressures.

One observation is that even if the deg10 results are situated between intact and deg25, the difference between intact and deg25 is much stronger compared to the difference between intact and deg10. In other words, the slip stability decay is not linear with the percentage of degradation. Moreover, in some velocity steps, we can see that *(a-b)* values of deg10 tests are equal or even a bit greater than the intact ones, but the values remain very close, thus it can be considered as due to experimental variability.

The value of the friction μ is, on the other side, not much affected by the dissolution (see Table 3. Values of the residual friction coefficient for different confining pressure and level of dissolution).

In fact, we can see that in the 600 kPa tests, the three peak values are nearly the same (μ=0.63–0.67), as well as the residual values (μ=0.22–0.25). The same happens in the 1 MPa tests where the peak is exactly the same and the intact residual value is only a bit higher that the degraded ones (μ=0.20). Finally, the 1.6 MPa run exhibits only a small difference in the value of the residual friction.

| | 600 kPa | 1 MPa | 1.6 MPa |
|---|---|---|---|
| **intact** | 0.24 | 0.24 | 0.26 |
| **dissolution 10%** | 0.21 | 0.20 | 0.21 |
| **dissolution 25%** | 0.24 | 0.20 | 0.19 |

*Table 3. Values of the residual friction coefficient for different confining pressure and level of dissolution*

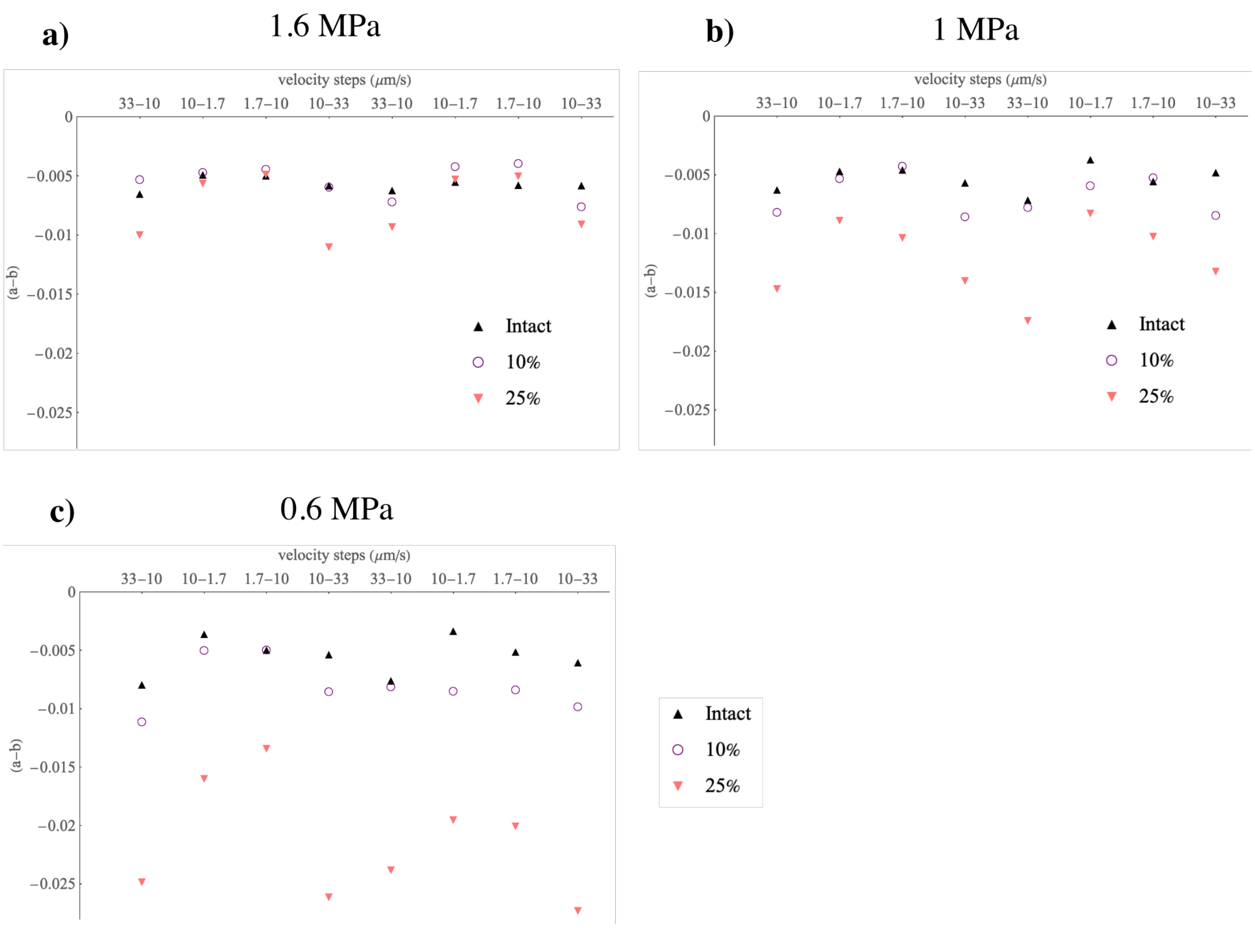


*Figure 5. Effect of the dissolution on the rate and state friction parameters (a-b) for the different velocity steps and for different confining stress.*

In Figure 6, we plot the values of the friction parameters *(a-b),* as a function of the confining pressure for the different degrees of dissolution. For the initial sand, the rate and state parameters are not affected by the confining stress but more by the velocity steps considered. The transition from 10 to 33 µm/s induces more weakening than the transition from 1.7 to 10 µm/s. This effect is also observed for the degraded sand. However, the sand that underwent 10% and 25% dissolution shows a clear effect of the confining stress on the rate and state parameters. for these tests, the *(a-b)* values get closer to zero when the confinement pressure is increased.

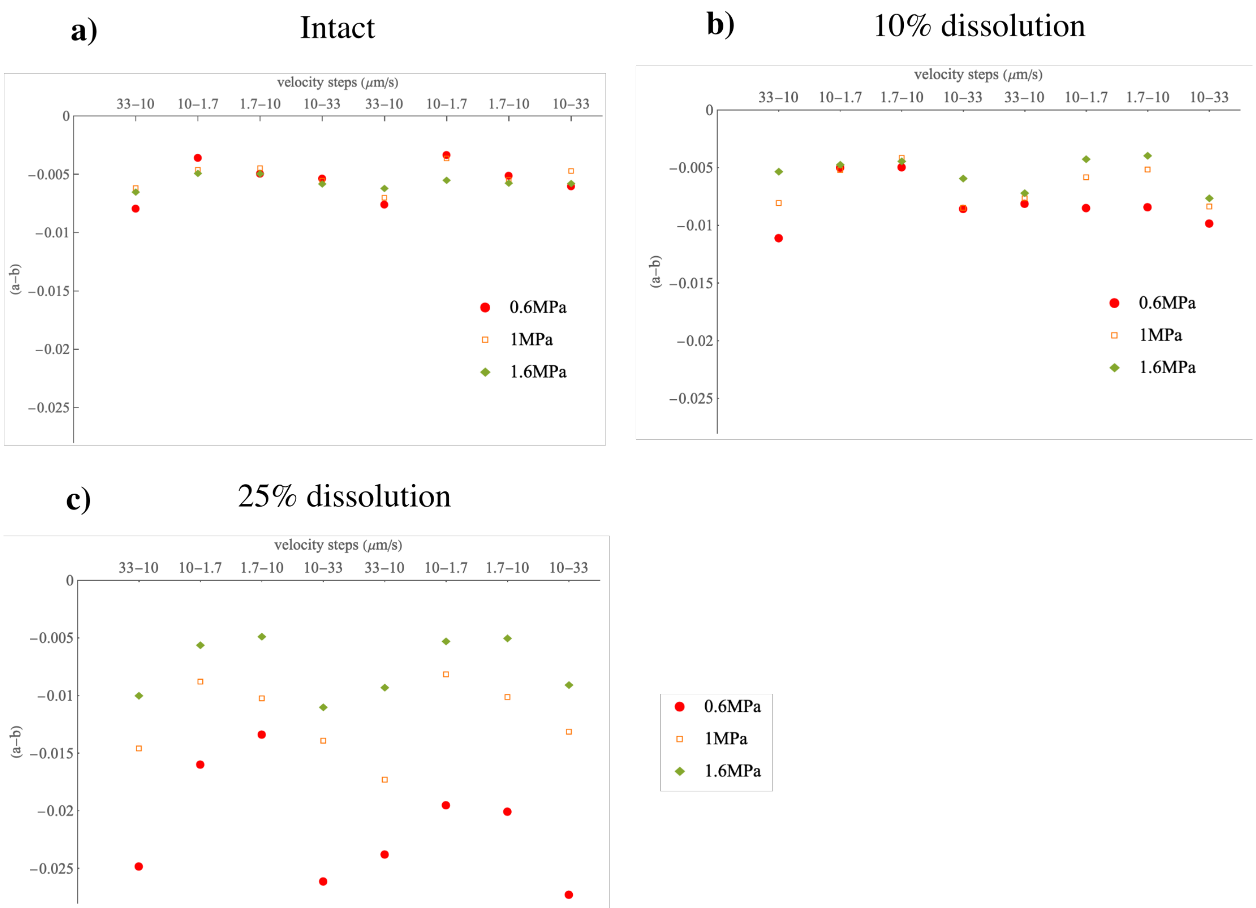


*Figure 6. Effect of the confining pressure on the rate and state friction parameters (a-b) for the different velocity steps and for different rate of dissolution.*

### 3.2. Particles roughness

The dissolution of the calcite through contact with an acid solution affects the grain size distribution but also the shape of the particles. The shape and in particular the roughness of the grains could influence the mechanical response of the sample (Anthony and Marone 2005). Thus, we characterize the roughness and shape of the particles using the specific BET surface area (SA

3100 BET surface area and pore size analyzer; Beckman Coulter, U.S.), sieves analysis and a Scanning Electron Microscope (SEM).

The roughness of a given sample is defined as the ratio between the surface areas obtained from the BET method and the particle size analysis (considering spherical particles). The BET method is a way to calculate the specific surface area of a sample based on gas adsorption. Nitrogen is pumped into the sample at a given pressure, with constant temperature (corresponding to the boiling point of liquid Nitrogen) and the adsorption process is measured volumetrically. The isotherm data obtained from this procedure enable to determine the specific surface area based on the theory developed by (Brunauer, Emmett, and Teller 1938). This value of the specific surface area is accurate and can be compared with one obtained from the particle size distribution (PSD). The latter is obtained by assuming that the mass of material obtained for each size correspond to spherical particles with the diameter of the mesh size (or the size of the volume equivalent for laser diffraction). The results are reported in Table 4.

| **Sample** | $S_{PSD}$ ($m^2/g$) | $S_{BET}$ ($m^2/g$) | **Rugosity** |
|---|---|---|---|
| Intact | $5.34\times10^{-2}$ | 0.96 | 18.03 |
| 10% | $3.29\times10^{-2}$ | 0.83 | 25.32 |
| 25% | $9.48\times10^{-3}$ | 0.99 | 104.32 |

*Table 4.Values of the specific surface area obtained from the BET method (SBET) or the particle size distribution (SPSD) and the rugosity for different level of dissolution*

The specific surface area obtained from the PSD exhibits a decrease with the dissolution. It is due to the elimination of the small particles that contributes substantially to the value of the specific surface. However, the values obtained from the BET method are not notably affected by the dissolution. Consequently, the roughness increases with the dissolution rate. To understand these results, observations of the grains have been performed using a Scanning Electron Microscope (FEI XL30 SEM) with variable pressure. The specimens have been coated with gold film prior to be placed in the microscope. Images of the intact sand and the sand with 25% degradation are shown in Figure 7. The intact sand exhibits much more fine particles attached to each other or to larger grains than the samples which experienced dissolution. Moreover, grains with a diameter larger than 10μm in the intact sand (Figure 7. b) present an external surface that is smoother than the one in the dissolved sand (Figure 7. d).

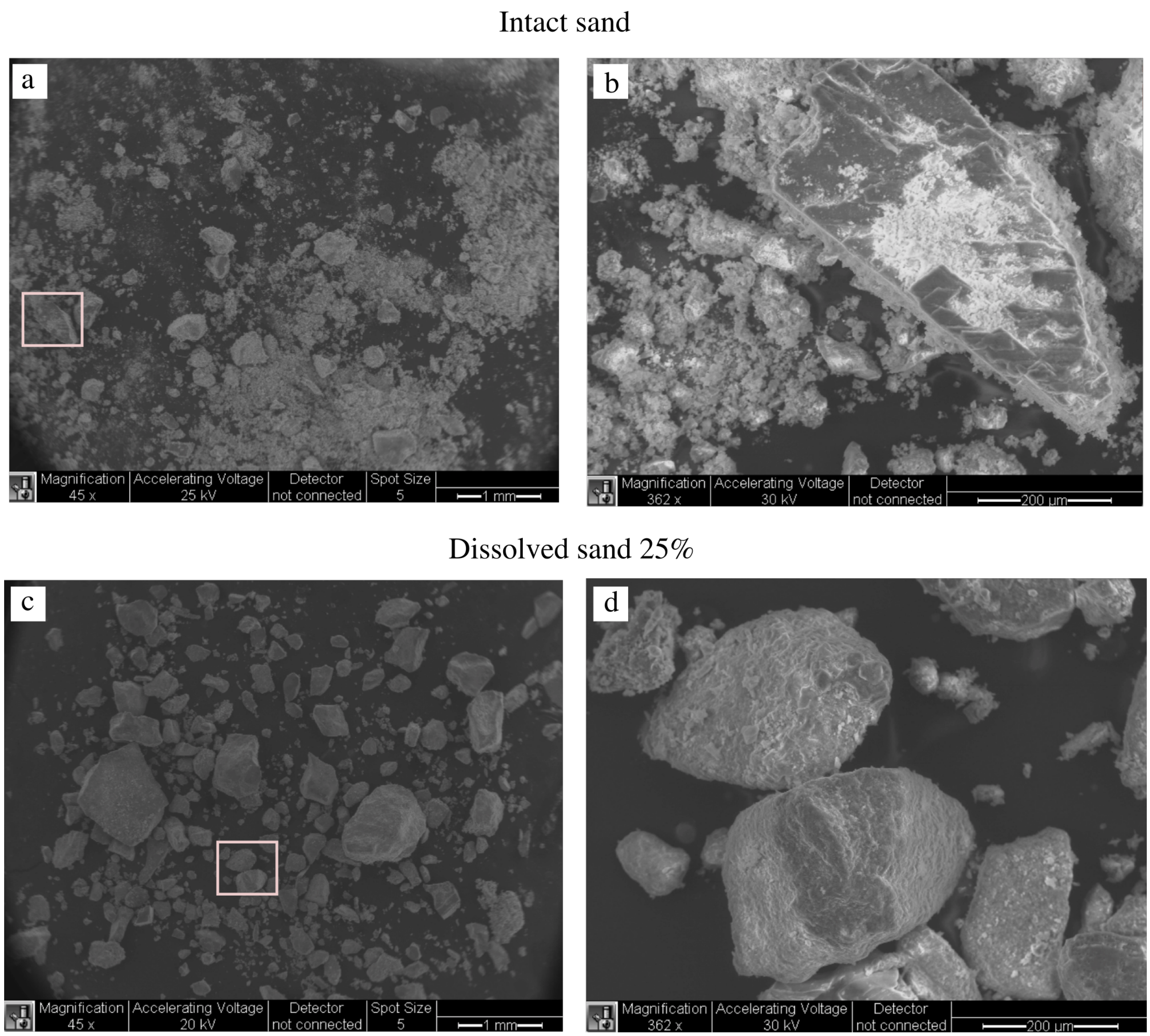


*Figure 7. Scanning Electron Microscope images of the intact sand (a and b), and the sand with 25% dissolution (c and d)*

## 4. Discussion and implications for potential fault reactivation due to acidic fluid injection

In this section, we integrate the mechanical data and the microstructural investigations from our experiments to discuss the role of the confining stress and the dissolution on the velocity weakening behavior of carbonate bearing faults. An empirical law is proposed to account for these phenomena on the rate and state friction parameters. This law is then used to determine in which conditions the injection of an acidic fluid could induced potential seismic slips in projects like carbon storage and acid gas disposals.

### 4.1. Empirical law for the evolution of rate and state friction parameters

Our results show that the mechanical behavior of simulated carbonate-bearing faults strongly depends on the applied normal stress and is modulated by the imposed slip velocity and the chemical dissolution of the grains, characterized by the fractal number of the grain size distribution.

A number of experimental studies have focused on the behavior of carbonate materials (Carpenter et al. 2016; Smith, Nielsen, and Di Toro 2015; Chen, Verberne, and Spiers 2015) under different range of temperature, velocities and confinement using double direct shear and rotary shear experiments. They observed a strong resistance and a friction coefficient at the peak between 0.6 and 0.7, consistent with our observations. However, the steady state friction coefficients they obtained in their experiments stay close to the peak value, exhibiting thus almost no weakening or strengthening. This discrepancy is due to the size of the sample used in the ACSA as explained in (Chambon, Schmittbuhl, and Corfdir 2006a). This macroscopic slip-weakening operating over decimetric distances is induced by a progressive mechanical decoupling between the interfacial layer and the bulk of the samples, as shown by image analysis during shearing.

Experiments conducted at typical velocities consistent with earthquake nucleation (a few micrometers per seconds like here) exhibits a velocity neutral or velocity strengthening behavior (Carpenter et al. 2016; Verberne et al. 2014) for normal stresses corresponding to those encountered in injection sites ($\sigma$ <20 MPa). The order of magnitude of the *(a-b)* coefficient*,* we have obtained ($10^{-2}$) is in agreement with previous studies on friction in gouge materials. Nevertheless, our experiments reveal a velocity weakening behavior. This weakening has also been observed by (Chambon 2003) for monodisperse quartz sand and glass beads. Friction in gouge material displays a peculiar behavior compared rock to rock interface. The latter exhibits a velocity softening for sub-seismic velocities whereas, the gouge a velocity strengthening (Chambon 2003). The difference comes from the volumetric variations in granular materials that can affect the shear behavior (Marone 1998; Beeler and Tullis 1997) and the large displacements applied in our experiments to the gouge before applying the velocity steps. The apparent friction is a gouge can be expressed as:

$$\mu = \mu_g + \frac{d\phi}{d\gamma} \tag{6}$$

where $\mu_g$ is the grain to grain friction and $\frac{d\phi}{d\gamma}$ is the volume change (dilatancy rate) with increasing shear displacement $\gamma$. In a granular assembly, even if the grain to grain friction is velocity weakening, the properties of the apparent friction is dominated by the dilatancy rate for the usual sizes of the sample. Yet, the rate of dilatancy increases with velocity (Marone, Raleigh, and Scholz 1990). (Chambon, Schmittbuhl, and Corfdir 2006b) have observed a low rate of volumetric variations with the ACSA. Therefore, in this device, the behavior of the gouge is controlled by the grain to grain friction, which explains the velocity weakening. The discrepancy between our results and previous studies is due to the difference of the samples' thickness.

In Figure 6, our results show an increase of the *(a-b)* parameter with the confining stress. This evolution is in agreement with the results of (Carpenter et al. 2016) for the shearing of powdered Carrara marble. They observed an increase of *(a-b)* for confining stresses below 50 MPa and then a decrease of this parameter. They argue that this change in the evolution is due to a transition from a brittle to a semi-brittle mechanism for the deformation of the gouge. We can plot (see **Error! Reference source not found.**) the evolution of the rate and state parameter *(a-b)* as a function of the confining stress for the different ratio of dissolution. The values for a given step is defined as the mean of the different values obtained and the error bars are estimated by the maximum deviation from the mean value of the different values of the coefficient obtained for the same velocity step in the same conditions. The evolution of the rate and state parameter is well described by a logarithmic law as follows:

$$(a - b) = A_1 \log\left(\frac{\sigma}{\sigma_0}\right) \tag{7}$$

where $\sigma_0$ is a reference confining stress, and $A_1$ is a parameter that depends on the velocity step considered. The experimental values and the evolution of the model with parameters obtained from a fitting with the least-squares method are represented together on Figure 8 for the velocity step 10-33 µm/s. The coefficient of determination exhibits values above 0.99 in all cases.

The analysis of the rugosity of the particles exhibit an increase with the dissolution. However, previous studies on simulated gouges have shown that an increase of the roughness in a frictional contact tends to induce a strengthening with velocity (Marone and Cox 1994; Anthony and Marone 2005). Therefore, the evolution of the rate-and-state parameters with the dissolution cannot be interpreted as an effect of the rugosity of the particles, but rather on the evolution of the particle size distribution. In the same way as the confining stress, we can plot the evolution of the rate and state parameter *(a-b)* as a function of the degree of dissolution, represented by the fractal number of the particle size distribution, for the different confining stresses (Figure 9). It is also well described by a logarithmic law as follows:

$$(a-b) = A_2 \log\left(\frac{D}{D_0}\right) \tag{8}$$

Where $D_0$ is a reference fractal number, and $A_2$ is a parameter that depends on the velocity step considered. These empirical laws enable to capture the evolution of the parameter (a-b) in our experiments, but previous studies have shown the triggering of complex multi-physical mechanisms with increasing velocities and normal stresses (Di Toro et al. 2011; Verberne et al. 2014; Carpenter et al. 2016) that would limit the application of this law. However, for conditions of the shallow crust ($\sigma <$20 MPa and T<100°C) and for velocities corresponding to the nucleation of a seismic slip, the mechanisms involved in the deformation of a gouge are the same as our experiments.

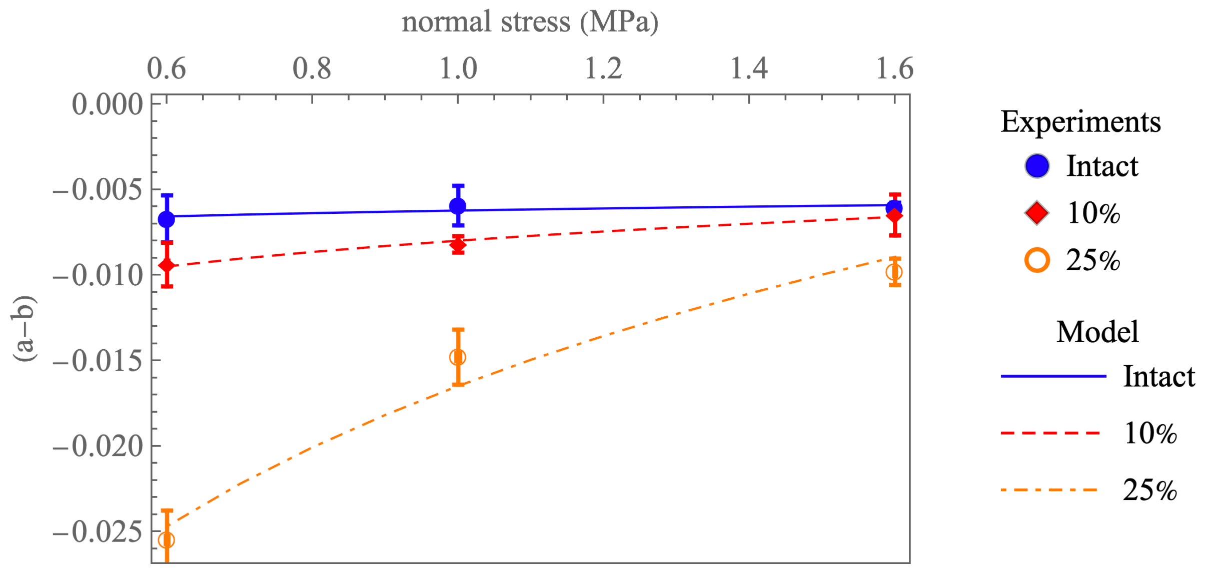


*Figure 8.Comparison of the model and the experimental data for the evolution of the rate and state parameters (a-b) as a function of the normal stress (velocity step 10-33 /s).*

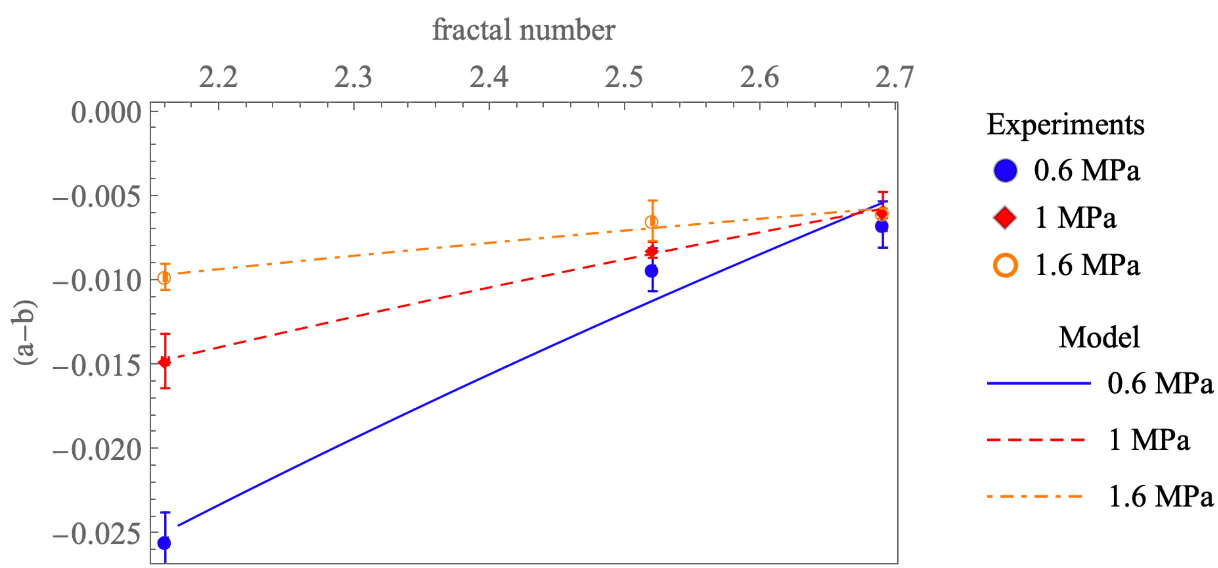


*Figure 9. Comparison of the model and the experimental data for the evolution of the rate and state parameters (a-b) as a function of the fractal number of the grain size distribution (velocity step 10-33 /s).*

### 4.2.Implications for fault reactivation

The study of carbonate bearing faults is of key importance as a great number of earthquakes are triggered in such lithologies. Noteworthy examples of seismic slips triggered and propagated through a fault composed of calcite are the magnitude 7.9 Wenchuan (China) earthquake in 2008 (Chen et al. 2013), the magnitude 6.2 Aigion (Greece) earthquake in 1995 (Bernard et al. 1997), or the magnitude 7.6 Chi-Chi (China) earthquake in 1999 (Boullier et al. 2009). Carbonate rocks are particularly ubiquitous in Italy and in the Apennines where the tectonic activity produce number of seismic events, like in the Amatrice and Norcia areas for the 2016-17 seismic sequence (Pizzi et al. 2017), or in L'Aquila for the 2009 earthquake (Valoroso et al. 2014). Moreover, many reservoirs in the world and potential sites for injection of CO2 storage or acid gas disposal are composed or carbonate materials (Bjorlykke 2010) and present faults that may induce leakage from the storage if they would be reactivated.

Sliding along an existing fault favors grain comminution and abrasion and thus, an increase of the fractal number (Storti, Billi, and Salvini 2003). Our results show that this increase of the fractal number would tend to stabilize the fault. On the other side, injection of an acid fluid tends to decrease this fractal number by dissolving the small grains. This dissolution would make the fault more velocity weakening and promote seismic slips. To determine in which conditions a fault located in a carbonate reservoir can be reactivated by a change in its frictional properties, we merge the two evolutions of the rate and state properties with the confining stress and the fractal number into a single law:

$$(a - b) = A_1 \log\left(\frac{\sigma}{\sigma_0}\right) + A_2 \log\left(\frac{D}{D_0}\right) \qquad (9)$$

The coefficient of determination for this law and the two velocity steps considered in our experiments are 0.95 and 0.98. We plot, in Figure 10, the value of *(a-b),* as a function of the normal stress and the fractal number. It enables us to define the region of stability for a fault in a carbonate reservoir.

In our experiments, the maximum ratio of mass decrease due to dissolution of calcite that we have considered is 25%. This value is similar to the decrease of calcite content obtained in (Bakker 2017) after 10,000 years, based on geochemical simulations of the long term effect of $CO_2$ on the mineral composition of a fault gouge, considering a residence time of 1000 years. In this study, the authors considered a carbonate bearing claystone and have investigated the effect of long-term exposure to $CO_2$ on the frictional properties of the fault by changing its mineral composition according to the geochemical model and different scenarios.

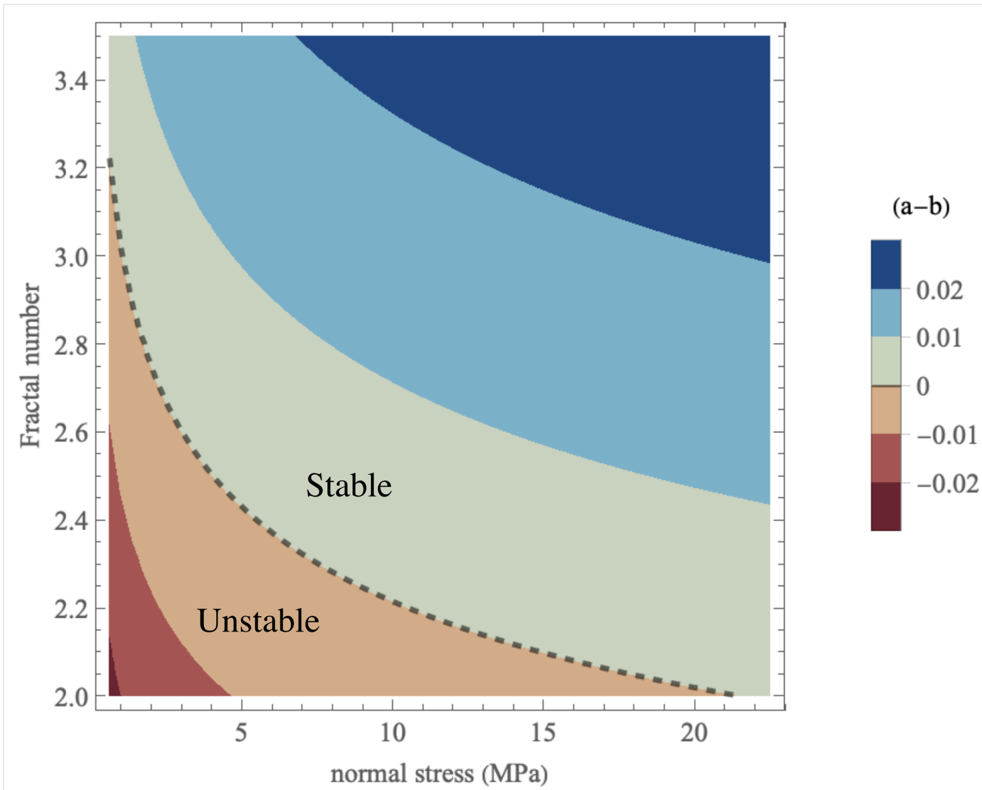


*Figure 10. Contours of the values of (a-b) as functions of the normal stress and the fractal number. The dashed line represents the limit between the velocity stable and unstable regions.*

The temperature plays also an important role in the values of the rate and state friction parameters. (Verberne et al. 2014) conducted velocity stepping experiments on carbonate materials at velocities similar to this study and highlighted the effect of temperature. From their experimental data on $CaCO_3$, we can interpolate the dependency of the $(a - b)$ parameter using a linear law between 20 and 100°C. This dependency of the rate and state parameter in temperature is then integrated into the previous logarithmic law (see Eq. 10).

$$(a - b) = A_1 \log\left(\frac{\sigma}{\sigma_0}\right) + A_2 \log\left(\frac{D}{D_0}\right) - A_3 T \tag{10}$$

Where $A_3$ is a parameter describing the influence of temperature on *(a-b)*. In Figure 11, we plot the diagram representing the limit of region of stability of the fault (*a-b=0*) considering the effect of temperature on the value of *(a-b)*. Compared to the previous limit of stability, the one that considers the effect of temperature is shifted upwards and it tends to destabilize the fault. The effect of temperature is integrated considering a geothermal gradient of 30°C/km and the normal stress at a given depth is calculated using a submerged unit weight of 15 kN/m$^3$. In this diagram, we also highlight the shallower depth of a $CO_2$ storage project, in order to keep the CO2 supercritical, which is 800 meters (Nakanishi et al. 2009) and the shallower depth of acid gas injection project in western Canada, which is 705 meters (Bachu and Gunter 2002). We observe that the injection of an acid in a reservoir can lower the fractal number by dissolving the small grains and reach a value around 2.16 if 25% of the mass is dissolved and the initial fractal number is close to the value of a self-similar distribution (2.6). In this case, the (a-b) parameter of a fault gouge can present a transition from positive to negative, and therefore, the fault can become unstable and slip seismically at typical depth considered for acid gas and carbon storage.

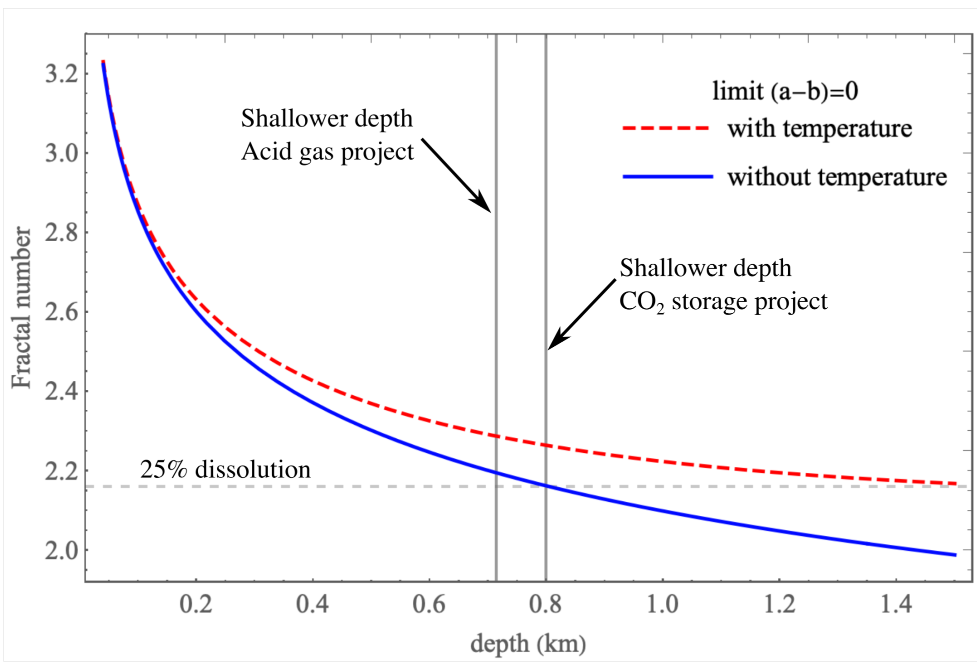


*Figure 11. Plot of the limits of the stable and unstable zone for the friction parameters obtained from the logarithmic law in the depth-fractal number space taking (or not) into account the effect of temperature on (a-b).*

## 5. Concluding remarks

In this paper, we investigate the effect of the injection of an acid fluid on the frictional properties of a fault located in a carbonate reservoir. The rate and state parameters *(a-b)* of a simulated calcite gouge are evaluated using an annular shear apparatus and conducting velocity stepping experiments. We observe that the long-term exposure to an acid fluid can weaken the fault by dissolving the small particles and changing the fractal number of the grain size distribution. Moreover, the *(a-b)* parameter increases with the normal stress applied to the fault. These two dependencies are described using a logarithmic law and it enables us to estimate that chemical reactions could be at the origin of a seismic slip in a storage site by changing the frictional properties of the fault.

## References


An, Lin Ji, and Charles G. Sammis. 1994. "Particle Size Distribution of Cataclastic Fault Materials from Southern California: A 3-D Study." *Pure and Applied Geophysics PAGEOPH* 143 (1–3): 203–27. https://doi.org/10.1007/BF00874329.

Anthony, Jennifer L., and Chris J. Marone. 2005. "Influence of Particle Characteristics on Granular Friction." *Journal of Geophysical Research B: Solid Earth* 110 (8): 1–14. https://doi.org/10.1029/2004JB003399.

Bachu, Stefan, and William D. Gunter. 2002. "Characteristics of Acid Gas Injection Operations in Western Canada. Interim Report to International Energy Agency - Greenhous Gas R&D Programme."

Bachu, Stefan, and William D. Gunter. 2004. "Acid-Gas Injection in the Alberta Basin, Canada: A C02-Storage Experience." In *Geological Storage of Carbon Dioxid*, edited by R. H. BAINES, S. J. & WORDEN, 225–34. Geological Society, London, Special Publications.

Baisch, Stefan, Robert Vörös, Elmar Rothert, Henrik Stang, Reinhard Jung, and Rüdiger Schellschmidt. 2010. "A Numerical Model for Fluid Injection Induced Seismicity at Soultz-Sous-Forets." *International Journal of Rock Mechanics and Mining Sciences* 47: 405–13. https://doi.org/10.1016/j.ijrmms.2009.10.001.

Bakker, Elisenda. 2017. "Frictional and Transport Properties of Simulated Faults in CO2 Storage Reservoirs and Clay-Rich Caprocks." *Utrecht Series in Earth Sciences №124*.

Beeler, N. M., and Terry E. Tullis. 1997. "The Roles of Time and Displacement in Velocity-Dependent Volumetric Strain of Fault Zones." *Journal of Geophysical Research : Solid Earth* 102 (B10): 22,595-22,609.

Bernard, P, P Briole, B Meyer, H Lyon-Caen, J-M Gomez, C Tiberi, C Berge, et al. 1997. "The Ms=6.2, June 15, 1995 Aigion Earthquake (Greece): Evidence for Low Angle Normal Faulting in the Corinth Rift." *Journal of Seismology* 1 (2): 131–50.

Bjorlykke, Knut. 2010. *Petroleum Geoscience: From Sedimentary Enviroments to Rock Physics*. *Petroleum Geoscience*. https://doi.org/10.1007/978-3-642-02332-3.

Boullier, Anne Marie, En Chao Yeh, Sébastien Boutareaud, Sheng Rong Song, and Chin Ho Tsai. 2009. "Microscale Anatomy of the 1999 Chi-Chi Earthquake Fault Zone." *Geochemistry,* *Geophysics, Geosystems* 10 (3). https://doi.org/10.1029/2008GC002252.

Brunauer, Stephen, P. H. Emmett, and Edward Teller. 1938. “Adsorption of Gases in Multimolecular Layers.” *Journal of the American Chemical Society* 60 (2): 309–19. https://doi.org/citeulike-article-id:4074706.

Cappa, Frederic. 2012. “Impact of CO2 Geological Sequestration on the Nucleation of Earthquakes.” *Geophysical Research Letters, 38, L17313, 2011*, September. http://escholarship.org/uc/item/15f9x6mp#page-12.

Carpenter, B M, C Collettini, C Viti, and A Cavallo. 2016. “The Influence of Normal Stress and Sliding Velocity on the Frictional Behaviour of Calcite at Room Temperature: Insights from Laboratory Experiments and Microstructural Observations.” *Geophysical Journal International* 205 (1): 548–61. https://doi.org/10.1093/gji/ggw038.

Chambon, Guillaume. 2003. “Caractérisation Expérimentale Du Frottement Effectif Des Zones de Faille.” École Nationale des Ponts et Chaussées. http://tel.archives-ouvertes.fr/tel-00006613/.

Chambon, Guillaume, Jean Schmittbuhl, and Alain Corfdir. 2006a. “Frictional Response of a Thick Gouge Sample: 1. Mechanical Measurements and Microstructures.” *Journal of Geophysical Research: Solid Earth* 111 (9): 1–17. https://doi.org/10.1029/2003JB002731.

Chambon, Guillaume, Jean Schmittbuhl, and Alain Corfdir. 2006b. “Frictional Response of a Thick Gouge Sample: 2. Friction Law and Implications for Faults.” *Journal of Geophysical Research: Solid Earth* 111 (9): 1–12. https://doi.org/10.1029/2004JB003339.

Chen, Jianye, Berend A Verberne, and Christopher J Spiers. 2015. “Effects of Healing on the Seismogenic Potential of Carbonate Fault Rocks: Experiments on Samples from the Longmenshan Fault, Sichuan, China.” *Journal of Geophysical Research : Solid Earth* 120 (8): 5479–5506. https://doi.org/10.1002/2015JB012051.Received.

Chen, Jianye, Xiaosong Yang, Shengli Ma, and Christopher J Spiers. 2013. “Mass Removal and Clay Mineral Dehydration/Rehydration in Carbonate-Rich Surface Exposures of the 2008 Wenchuan Earthquake Fault : Geochemical Evidence and Implications for Fault Zone Evolution and Coseismic Slip.” *Journal of Geophysical Research : Solid Earth* 118 (2): 474–96. https://doi.org/10.1002/jgrb.50089.

Collettini, Cristiano, C. Cardellini, G. Chiodini, N. De Paola, R. E. Holdsworth, and Steven A. F. Smith. 2008. “Fault Weakening Due to CO2 Degassing in the Northern Apennines: Short- and Long-Term Processes.” *Geological Society, London, Special Publications* 299 (1): 175–94. https://doi.org/10.1144/SP299.11.

Dieterich, James H. 1981. “Constitutive Properties of Faults with Simulated Gouge.” *Geophysical Monograph Series* 24: 103–20. http://www.agu.org/books/gm/v024/GM024p0103/GM024p0103.shtml.

Ellsworth, William L. 2013. “Injection-Induced Earthquakes.” *Science* 341 (July): 1–8.

Espinoza, D Nicolas. 2011. “Carbon Geological Storage – Underlying Phenomena and

Implications –."

Khan, Chawarwan, Robert Amin, and Gary Madden. 2013. "Effects of CO2 and Acid Gas Injection on Enhanced Gas Recovery and Storage." *Journal of Petroleum Exploration and Production Technology* 3 (1): 55–60. https://doi.org/10.1007/s13202-012-0044-8.

Koval, Georg, François Chevoir, Jean-Noël Roux, Jean Sulem, and Alain Corfdir. 2011. "Interface Roughness Effect on Slow Cyclic Annular Shear of Granular Materials." *Granular Matter* 13 (5): 525–40. https://doi.org/10.1007/s10035-011-0267-2.

Marone, Chris J. 1998. "Laboratory-Derived Friction Laws and Their Application To Seismic Faulting." *Annual Review of Earth and Planetary Sciences* 26 (1): 643–96. https://doi.org/10.1146/annurev.earth.26.1.643.

Marone, Chris J., and S. J. D. Cox. 1994. "Scaling of Rock Friction Constitutive Parameters: The Effects of Surface Roughness and Cumulative Offset on Friction of Gabbro." *Pure and Applied Geophysics* 143 (1): 359–85.

Marone, Chris J., C Barry Raleigh, and Christopher H. Scholz. 1990. "Frictional Behavior and Constitutive Modeling of Simulated Fault Gouge." *Journal of Geophysical Research : Solid Earth* 95 (B5): 7007–25.

Messen, Y. H., A. Corfdir, and J. Schmittbuhl. 2013. "Mechanical Healing of Simulated Fault Gouge." *Geophysical Journal International* 193 (1): 252–62. https://doi.org/10.1093/gji/ggs082.

Mortezaei, Kimia, and Farshid Vahedifard. 2015. "Numerical Simulation of Induced Seismicity in Carbon Capture and Storage Projects." *Geotechnical and Geological Engineering* 33 (2): 411–24. https://doi.org/10.1007/s10706-015-9859-7.

Nakanishi, Shigetaka, Yasunobu Mizuno, Tadahiko Okumura, Hideaki Miida, Takumi Shidahara, and Shin-ichi Hiramatsu. 2009. "Methodology of CO2 Aquifer Storage Capacity Assessment in Japan and Overview of the Project." *Energy Procedia* 1 (1). Elsevier: 2639–46. https://doi.org/10.1016/j.egypro.2009.02.031.

Pizzi, A., A. Di Domenica, F. Gallovic, L. Luzi, and R. Puglia. 2017. "Fault Segmentation as Constraint to the Occurrence of the Main Shocks of the 2016 Central Italy Seismic Sequence." *Tectonics* 36 (11): 2370–87. https://doi.org/10.1002/2017TC004652.

Rattez, Hadrien, Ioannis Stefanou, and Jean Sulem. 2018. "The Importance of Thermo-Hydro-Mechanical Couplings and Microstructure to Strain Localization in 3D Continua with Application to Seismic Faults. Part I: Theory and Linear Stability Analysis." *Journal of the Mechanics and Physics of Solids* 115: 54–76. https://doi.org/10.1016/j.jmps.2018.03.004.

Rattez, Hadrien, Ioannis Stefanou, Jean Sulem, Manolis Veveakis, and Thomas Poulet. 2018. "The Importance of Thermo-Hydro-Mechanical Couplings and Microstructure to Strain Localization in 3D Continua with Application to Seismic Faults . Part II : Numerical Implementation and Post-Bifurcation Analysis." *Journal of the Mechanics and Physics of Solids* 115: 1–29. https://doi.org/10.1016/j.jmps.2018.03.003.

Rattez, Hadrien, Ioannis Stefanou, Manolis Veveakis, Thomas Poulet, and Jean Sulem. 2018. "Numerical Analysis of Strain Localization in Rocks with THM Couplings: Benchmark Tests and Microstructure." *Rock Mechanics and Rock Engineering*.

Reid, Harry F. 1910. "The Mechanism of the Earthquake." In *The California Earthquake of April 18, 1906, Report of the State Earthquake Investigation Commision, Vol. 2*, 1–192.

Rice, James R., and A Ruina. 1983. "Stability of Steady Frictional Slipping." *Journal of Applied Mechanics* 50 (2): 343. https://doi.org/10.1115/1.3167042.

Rubinstein, Justin L., and Alireza Babaie Mahani. 2015. "Myths and Facts on Wastewater Injection, Hydraulic Fracturing, Enhanced Oil Recovery, and Induced Seismicity." *Seismological Research Letters* 86 (4): 1060–67. https://doi.org/10.1785/0220150067.

Ruina, A. 1983. "Slip Instability and State Variable Friction Laws." *Journal of Geophysical Research: Solid Earth* 88 (12): 10,359-10,370. http://onlinelibrary.wiley.com/doi/10.1029/JB088iB12p10359/full.

Sammis, Charles G., Geoffrey King, and Ronald L. Biegel. 1987. "The Kinematics of Gouge Deformation." *Pure and Applied Geophysics* 125 (5): 777–812. https://doi.org/10.1007/BF00878033.

Samuelson, Jon E, and Christopher J Spiers. 2012. "Fault Friction and Slip Stability Not Affected by CO2 Storage : Evidence from Short-Term Laboratory Experiments on North Sea Reservoir Sandstones and Caprocks." *International Journal of Greenhouse Gas Control* Volume 11 (November 2012): 78–90.

Schoenball, Martin, and William Ellsworth. 2017. "A Systematic Assessment of the Spatiotemporal Evolution of Fault Activation Through Induced Seismicity in Oklahoma and Southern Kansas." *Journal of Geophysical Research : Solid Earth* 122 (12): 10,189-10,206. https://doi.org/10.1002/2017JB014850.

Scholz, Christopher H. 1998. "Earthquakes and Friction Laws." *Nature* 391 (January 1998): 37–42.

Smith, Steven A. F., Stefan Nielsen, and Giulio Di Toro. 2015. "Strain Localization and the Onset of Dynamic Weakening in Calcite Fault Gouge." *Earth and Planetary Science Letters* 413 (March): 25–36. https://doi.org/10.1016/j.epsl.2014.12.043.

Steacy, S J, and C G Sammis. 1991. "An Automaton for Fractal Patterns of Fragmentation." *Nature* 353 (6341): 250–52. https://doi.org/10.1038/353250a0.

Storti, Fabrizio, Andrea Billi, and Francesco Salvini. 2003. "Particle Size Distributions in Natural Carbonate Fault Rocks : Insights for Non-Self-Similar Cataclasis." *Earth and Planetary Science Letters* 206: 173–86.

Tembe, Sheryl, David A. Lockner, and Teng Fong Wong. 2010. "Effect of Clay Content and Mineralogy on Frictional Sliding Behavior of Simulated Gouges: Binary and Ternary Mixtures of Quartz, Illite, and Montmorillonite." *Journal of Geophysical Research: Solid*

*Earth* 115 (3): 1–22. https://doi.org/10.1029/2009JB006383.

Toro, Giulio Di, Takehiro Hirose, Stefan Nielsen, Giorgio Pennacchioni, and Toshihiko Shimamoto. 2011. “Natural and Experimental Evidence During Earthquakes.” *Science* 3011 (2006): 647–49. https://doi.org/10.1126/science.1121012.

Unterreiner, P., P. Lerat, I. Vardoulakis, F. Schlosser, E. De Laure, and G. Belmont. 1993. Brevet sur l’Appareil de Cisaillement Simple Annulaire (ACSA), issued 1993.

Valoroso, Luisa, Lauro Chiaraluce, Cristiano Collettini, Istituto Nazionale, Vigna Murata, Dipartimento Scienze, Sapienza Università, and Piazzale Aldo Moro. 2014. “Earthquakes and Fault Zone Structure.” *Geology* 42 (4): 343–46. https://doi.org/10.1130/G35071.1.

Verberne, B. A., Christopher J Spiers, André R Niemeijer, J. H P De Bresser, D. A M De Winter, and O. Plümper. 2014. “Frictional Properties and Microstructure of Calcite-Rich Fault Gouges Sheared at Sub-Seismic Sliding Velocities.” *Pure and Applied Geophysics* 171 (10): 2617–40. https://doi.org/10.1007/s00024-013-0760-0.

Wilson, M. P., G. R. Foulger, J. G. Gluyas, R. J. Davies, and B. R. Julian. 2017. “*HiQuake* : The Human-Induced Earthquake Database.” *Seismological Research Letters* 88 (6): 1560–65. https://doi.org/10.1785/0220170112.

Yarushina, Viktoriya M., and David Bercovici. 2013. “Mineral Carbon Sequestration and Induced Seismicity.” *Geophysical Research Letters* 40 (5): 814–18. https://doi.org/10.1002/grl.50196.

Yehya, Alissar, Zhuo Yang, and James Robert Rice. 2018. “Effect of Fault Architecture and Permeability Evolution on Response to Fluid Injection.” *Journal of Geophysical Research: Solid Earth* 123 (11): 9982–97. https://doi.org/10.1029/2018JB016550.

Zoback, Mark D, and Steven M Gorelick. 2012. “Earthquake Triggering and Large-Scale Geologic Storage of Carbon Dioxide.” *Proceedings of the National Academy of Sciences of the United States of America* 109 (26): 10164–68. https://doi.org/10.1073/pnas.1202473109.